[9] Study of the diffraction grating on a convex surface as a dispersive element

S.V. Karpeev, S.N. Khonina, S.I. Kharitonov
Image Processing Systems Institute, Russian Academy of Sciences, Samara, Russia
Samara State Aerospace University, Samara, Russia

Abstract

A dispersive element in the form of the diffraction grating on a convex mirror surface is investigated. The groove profile of the grating is measured and the intensity distribution between the diffraction orders is calculated as a function of wavelength for the visible spectrum. Optomechanical elements for the required alignments of the spectrometer elements are designed and fabricated. Adjustment of a prototype optical scheme is implemented and point images for three monochromatic incident wavelengths are obtained. The energy distribution between the diffraction orders and the intensity maxima positions are in agreement with the simulation results.

Keywords: SPECTROMETER, GROOVE PROFILE, ENERGY DISTRIBUTION BETWEEN THE DIFFRACTION ORDERS, ADJUSTMENT OF A PROTOTYPE OPTICAL SCHEME.

Citation: KARPEEV S.V. STUDY OF THE DIFFRACTION GRATING ON A CONVEX SURFACE AS A DISPERSIVE ELEMENT / KARPEEV S.V., KHONINA S.N., KHARITONOV S.I. // COMPUTER OPTICS. – 2015. – VOL. 39(2). – P. 211-217

Introduction

The most advanced spectrometers to be used in small spacecrafts (SC) are the imaging spectrometers in Offner configuration [1–5]. Main advantages of these spectrometers are their compact sizes and possibility to lowly reduce chromatic aberrations and distortion. As a simplest base case, the Offner spectrometer shall contain two concentric mirrors. A diffraction grating on a mirror surface is used as a dispersive element. Usage of the diffraction grating allows us to achieve smaller sizes and smaller chromatic aberrations. Modeling the spectrometer performance [6–8] has confirmed high characteristics of images obtained by spectroscopic instruments.

The most sophisticated in implementation element of the spectroscopic instrument is the diffraction grating of a spectrograph fabricated on a mirror surface, in our case on a convex spherical mirror surface. Basic techniques for fabricating such gratings are the grooving using a special ruling machine and the holographic lithography. In Russia, both of these technologies are represented in the 'State Institute for Applied Optic' Scientific Production Association (Kazan) which is a part of Shvabe holding company. It is reasonable at the stage of prototyping to use, as an image-forming lens, a household telephotographic lens with proper optical characteristics, since prototype tests are performed for the visible wavelength spectrum. For the visible wavelength range (430–630 nm) such lens would completely replace an ad hoc lens designed for the spectrometer [6,7].

1. Fabricating and investigating the spectrometer grating

There are various control methods to control power distribution in diffraction orders for the diffraction gratings. For example, we can obtain arbitrary distributions for binary gratings thus forming quasi-periodic phase functions by overlapping the diffraction gratings [9]. The binary gratings are the easiest to manufacture using lithographic techniques, but they can produce only symmetrical orders, so their energy efficiency is limited. The largest energy efficiency concentrated in a diffraction order is provided by gratings with triangular profiles (the "blazed" gratings), but they are the most technologically sophisticated. This section will be particularly dedicated to discussing advantages and disadvantages of various types of diffraction gratings with due regard to their technology implementation.

The 'State Institute for Applied Optics' Scientific Production Association has all necessary equipment and expertise in manufacturing convex and

concave diffraction gratings [10]. For spatial frequencies of dozens of lines per millimeter, which should be implemented for the designed spectrometer, the grooving technique is the most suitable.

As was mentioned above, the most suitable is the grating with the triangular profile; however, the manufacturer has no opportunity to keep a set of cutters for a large spectrum of spatial frequencies; therefore, the profile form may be implemented in this company only by means of designated approximation within a proper zone. The measurement result of one of the actual grating profiles on the microinterferometer Zygo New View 7000 is given in Fig. 1.

It may be concluded from this figure that for the visible spectrum the profile has the height which considerably exceeds the optimum height of the reflecting grating $\lambda/4$. However, this high profile can provide necessary results, if the height corresponds to the phase progression by module $n\varpi$ for respective wavelengths. Thus, preliminary numerical investigation is required for the actual grating profile. It is evident that the investigation consists in calculating the Fourier decomposition (for the light amplitude distribution in diffraction orders) of phase functions corresponding to the investigated profiles for different wavelengths.
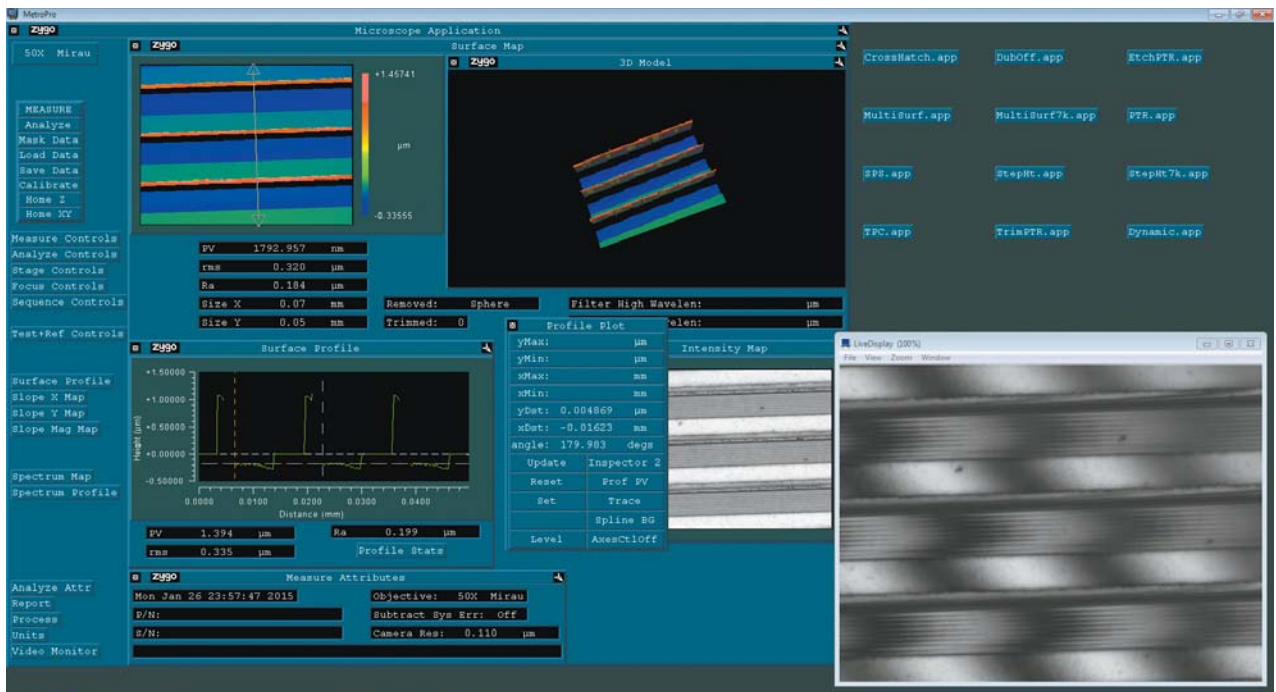
*Fig. 1. View of a program window when measuring
the profile of the diffraction grating on a mirror surface*

The manufacturer has presented three profile prototypes on two grating samples, moreover, on one of these gratings (grating 1) there were two sections performed with different profiles, one of which was obtained by means of additional liquid etching of the grooved profile. The profile graphs obtained by processing the measurements performed by the microinterferometer are given in Fig. 2. Here the profile of Fig. 2a corresponds to a non-etched section of the grating 1, the profile in Fig. 2b – to the etched section, and the profile in Fig. 2c – to the grating 2. It can be seen that the etching (profile in Fig. 2b) has resulted in removing a tooth about 2 µm in

height being present on the non-etched profile. Besides, there appeared some significant noises – the etching seemed to be non-isotropic. And the etched section has visually a slightly matt surface. The modeling results of light diffraction for different wavelengths on three measured profiles are given in Fig. 3 in the same order as the profiles in Fig. 2. Except the results for actual profiles, Fig. 3d shows the result for the ideal rectangular profile 0.13 µm in height. This figure shows that the actual profile in Fig. 4b may be considered as the approximation of the rectangular profile 0.5ϖ in height for the center wavelength.
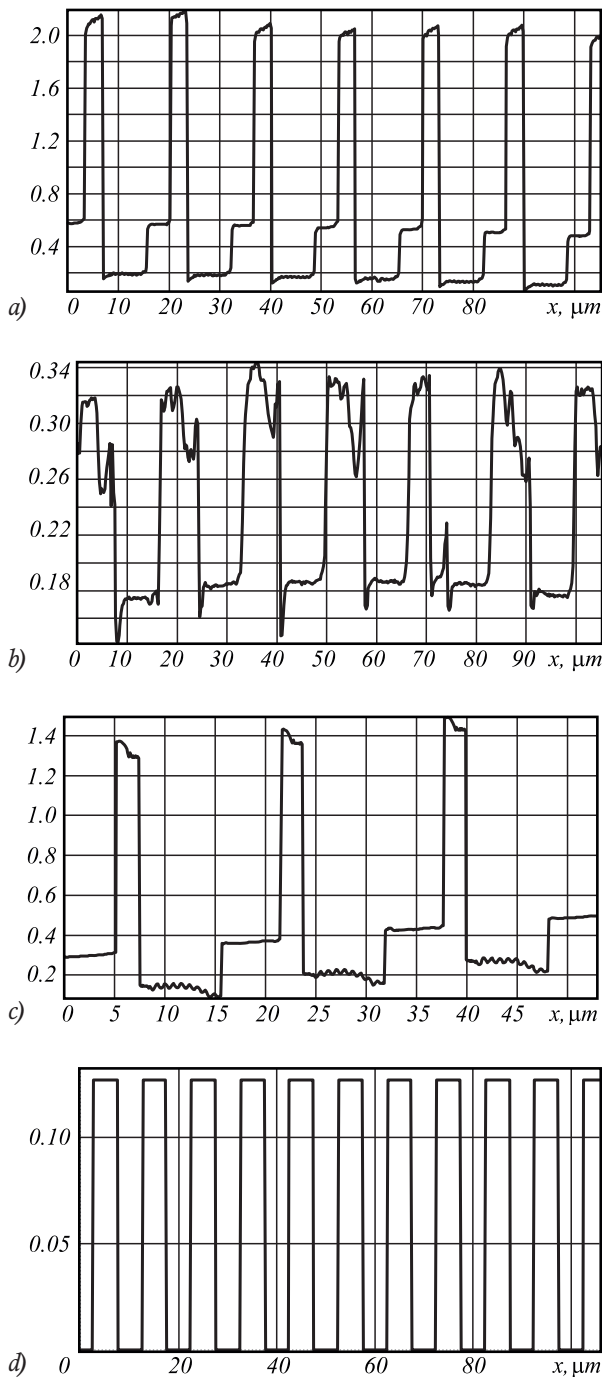
Fig. 2. View of the reflecting grating profiles

Fig. 3. The order distribution in the focal plane: for radiation 440 nm (dotted line), 540 nm (dashed line), 640 nm (full line), for the corresponding profiles in Fig. 2

The modeling results show the significant asymmetry in a diffraction pattern between +1 and −1 orders, especially for the profiles in Fig. 2*a* and Fig. 2*c*. This may be explained with the asymmetric grating profile. The efficiency for various wavelengths essentially depends on the grating profile form, provided that the first working order for different gratings is on opposite sides of an optical axis. At average, the efficiency in the first order varies over the range of 15 – 35 % for different wavelengths.

Full-scale experiments performed by means of a power meter showed the results which are close to the rated findings. It is not possible to exactly compare these results, because the regions, where the profile and the light flare were measured, may significantly vary in sizes when measuring the power and the grating profile may differ

in aperture that will be explained later. If we evaluate the modeling results as a whole, then, in our opinion, the profile in Fig. 2*b* shall show the best result. However, the usage of the grating with such a profile is complicated by the fact that the etching was performed only for a half square of the grating. The boundary between the etched and non-etched areas is perpendicular to the grooves and it is not sharp; therefore, the spectra properties will vary in slit height and hence in image aperture. This effect is clearly demonstrated in the next section based on distribution of the experimental intensity obtained during the spectrometer adjustment.

2. Mounting and adjustment of the spectrometer optical scheme

A schematic diagram of the spectrometer optical scheme with all necessary dimensions and allowances is given in Fig. 4.

Its main difference from the system computed in [6, 7] is the replacement of the standard lens to the domestic photolens "Jupiter – 21M" intended for Zenit-type cameras. This lens has its basic parameters (i.e. the light-gathering power and the focal distance) similar to the standard lens parameters. The spectrometer grating was fabricated and purchased in the 'State Institute for Applied Optics' Scientific Production Association completed with the mirror. The spectrometer slit 15 µm in width was manufactured as a chrome mask by means of an optical plotter CLWS-200. The CCD-camera has 2048×1526 pixels, the size of a sensible area is 5×6.55 mm, the pixel's size is 3.5 µm. While testing a prototype model, such small pixel size allows us to examine an aberration image in great detail.

Fig. 4. The spectrometer's optical system

While manufacturing optomechanical devices on a production line basis, the required installation accuracy of elements is provided by precise fabricating a mechanical structure supplied with optic holders. And only for the elements, which are the most crucial in terms of their installation accuracy, some additional alignments of mounting elements are required during mounting and alignment. Fig. 4 shows that installation tolerances for major scheme elements shall not exceed 0.06–0.1 mm of the linear error and 52' of the angle error. It was not possible to ensure such accuracies during manufacture of mechanical parts of the prototype model, so all elements of the optical system were mounted on a common plate-base made of duralumin 8 mm in thickness with holders on optomechanical adjusting devices manufactured by Standa. These devices could provide

transverse displacement of the slit, adjustment of the spherical mirror along the optical axis and in height, adjustment of the grating across and along the optical axis and, finally, adjustment of the CCD-matrix along and across the optical axis. The above mentioned displacements combined with the standard lens focusing enables to completely implement all degrees of freedom to adjust relationships of the scheme elements.

The main purpose of the first test step was to obtain the image of a monochromatic optical point source for various wavelengths. This objective becomes realistic if there is a wide-range reconfigurable laser system EKSPLA NT-200. This laser beam is astigmatic. To improve the beam we used spatial filtration in the point source with 20× microlens and 40 µm pinhole aperture. However, the image spot in output of the point source has an elliptic shape just

the same. It has been experimentally found out that a focal spot of the lens "Jupiter 21M", when lighting by means of a collimated beam from this source, becomes symmetrical only in beam masking until the aperture ratio is 1:16. When the mask is opened, the beam becomes elliptic and exposes the slit edges to light. We can also see a slit image in CCD. What is important is that the slit is located parallel to the grating grooves and its defocused image, being a strip, falls down almost at the whole grooves length. Therefore, after the grating we can see various energy distributions between orders in the defocused image corresponding to different parts of the grating (the profiles in Fig. 2a and Fig. 2b). Fig. 5 shows the respective intensity distributions for three wavelengths −430 nm (blue, Fig. 5a), 530 nm (green, Fig. 5b) and 630 nm (red, Fig. 5c). The most obvious is the distribution (Fig. 5a) where there are zero, +1 and −1 diffraction orders. The left part of the figure shows how the zero order disappears and +1 and −1 orders remain roughly the same that corresponds to the results shown in Fig. 3b. This part of the grating has the same profile type as in Fig. 2b. Whereas the right part shows the asymmetry in distribution between +1 and −1 orders that corresponds to the profile in Fig. 2a. Similar patterns can be observed either for green (Fig. 5b) and red (Fig. 5c). In view of the grating dispersion properties, one of the first orders goes here far beyond the range of the field of the CCD-matrix, and the upper order in the figures is zero.

These images are intended for tests only and do not require any precise adjustment of the scheme. To obtain working images of the point we have installed the second grating (profile in Fig. 3c). The scheme adjustment was carried out using a stopped-down lens. First, the lens was focused in the slit plane, and the slit and obtained point image were overlapped. We tried to get a round image spot after passing through the slit without diffraction fringes which showed that there was a light appeared on slit edges. Further alignment of the optical system included sequential control of element positions in the direction of light rays to achieve an aberration-free point image. Point images have been obtained for different colors. Fig. 6a shows an enlarged pattern of the point aberration image in blue. The maximum sizes over the level 0.5 in the aberration image are 4×4 pixels, i.e. about 15 µm, that corresponds to the slit width 15 µm and to the rated resolution of the "Jupiter-21M" lens. Hence, we may conclude that there are no resolution losses in the spectrometer.
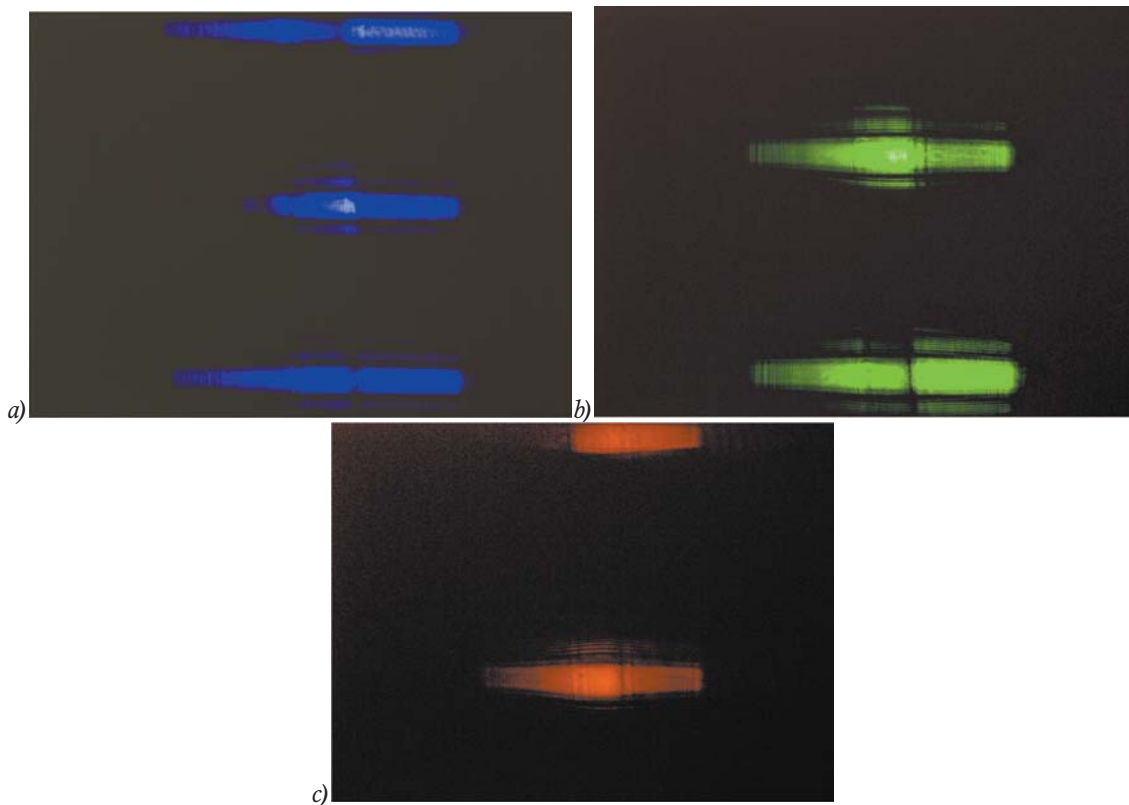
Fig. 5. Analysis of the intensities for different grating types
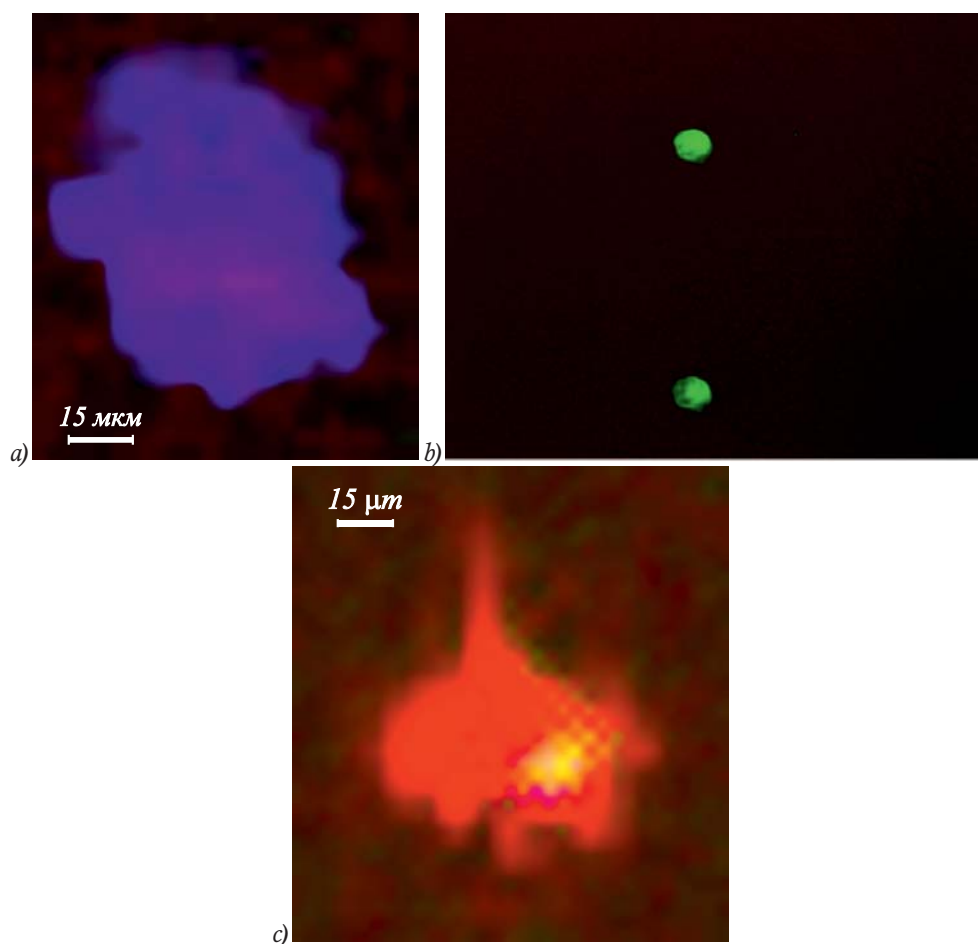
Fig. 6. The point images in different colors

For green points (Fig. 6*b*) the defocused image is given for the first working order which is placed at the bottom of the figure. We can see the relationship of the intensities approximately corresponding to Fig. 3*c* and even the edges of aperture blades that proves the correct lens adjustment at infinity. The figure also gives the point aberration image in red (Fig. 6*c*). The first-order image is twice more intensive here than in the zero order that is corresponding to the simulation results. The view of the aberration image is slightly worse than for blue, but if we consider the maximum sizes, they will be approximately the same. The flare light round the maximum becomes just better seen because the total intensity has been increased and not any light intensity correction was carried out at all.

The measured distance between blue and red point images in the first diffraction order is about 1300 μm which is corresponding to the calculation and simulation results.

Conclusion

The drawings have been developed and all basic mirror structures of the spectrometer have been manufactured, including the diffraction grating on the convex spherical surface. The groove profile of the grating is measured and the intensity distribution between the diffraction orders is calculated as a function of wavelength for the visible spectrum. Optomechanical elements for the required alignments of the spectrometer elements have been designed and fabricated. Adjustment of the prototype optical scheme has been implemented and point images for three monochromatic incident wavelengths have been obtained. The energy distribution between the diffraction orders and the intensity maxima positions are in agreement with the simulation results. The obtained resolution corresponds to the rated resolution of the imaging lens.

References

▎**1.** Mouroulis, P, Sellar, RG, Wilson, DW, Shea, JJ, Green, RO. Optical design of a compact imaging spectrometer for planetary mineralogy. Optical Engineering, 2007; 46 (6): 063001.

▎**2.** Mouroulis, P, Wilson, DW, Maker, PD, Muller, RE. Convex grating types for concentric imaging spectrometers. Applied Optics, 1998; 37 (31): 7200-7208.

▎**3.** Prieto-Blanco, X, Montero-Orille, C, Couce, B, de la Fuente, R. Analytical design of an Offner imaging spectrometer. Optics Express, 2006; 14 (20): 9156-9168.

▎**4.** Prieto-Blanco, X, Montero-Orille, C, Gonzalez-Nuez, H, Mouriz, MD, Lago, EL, de la Fuente, R. The Offner imaging spectrometer in quadrature. Optics Express, 2010; 18 (12): 12756-12769.

▎**5.** Lee, JH, Jang, TS, Yang, H-S, Rhee S-W. Optical Design of a Compact Imaging Spectrometer for STSAT3. Journal of the Optical Society of Korea, 2008; 12 (4): 262-268.

▎**6.** Kazanskiy, NL, Kharitonov, SI, Karsakov, AV, Khonina SN. Modeling action of a hyperspectrometer based on the Offner scheme within geometric optics. Computer Optics, 2014; 38 (2): 271-280.

▎**7.** Doskolovich, LL, Bezus, EA, Bykov DA. On the compensation of the diffraction orders overlap effect in the Offner spectrometer. Computer Optics, 2014; 38 (4): 777-781.

▎**8.** Kazanskiy, NL, Kharitonov, SI, Doskolovich, LL, Pavelyev AV. Modeling the performance of a spacebarne hyperspectrometer based on the Offner scheme. Computer Optics, 2015; 39 (1): 70-76.

▎**9.** Berezny, AE, Karpeev, SV, Uspleniev, GV. Computer-generated holographic optical elements produced by photolithography. Optics and Lasers in Engineering, 1991; 15 (5): 331-340.

▎**10.** Znamenskyi, MYu, Lukashevich, YaK, Skochilov, AF, Fedulova, NA. Transmissive threaded diffraction gratings for ultraviolet, visible and infrared regions of the spectrum. Journal of Optical Technology, 2014; 3: 51-54.

COMPUTER OPTICS